

# Catalytic Oxidation of Aniline to Azoxybenzene Over $\text{CuCr}_2\text{O}_4$ Spinel Nanoparticle Catalyst

Shankha S. Acharyya, Shilpi Ghosh, and Rajaram Bal\*

Catalytic Conversion Process Division, CSIR-Indian Institute of Petroleum, Dehradun 248005, India

## S Supporting Information

**ABSTRACT:** Cationic surfactant cetyltrimethylammonium chloride-mediated hydrothermal preparation of  $\text{CuCr}_2\text{O}_4$  spinel nanoparticles has been reported. This  $\text{CuCr}_2\text{O}_4$  spinel nanoparticle catalyst has been characterized by XRD, XPS, SEM, TEM, TGA, and ICP-AES. Characterization results showed the formation of  $\text{CuCr}_2\text{O}_4$  spinel nanoparticles with sizes between 25 and 50 nm. It was found that the catalyst can selectively convert aniline to azoxybenzene with  $\text{H}_2\text{O}_2$  as oxidant. The effect of different reaction parameters like reaction temperature,  $\text{H}_2\text{O}_2$  to aniline molar ratio, reaction time, and so forth have been studied in detail. An aniline conversion of 78% with azoxybenzene selectivity of 92% can be achieved over this catalyst at 70 °C. The catalyst did not show any leaching up to five reuses, showing the true heterogeneity of the catalyst. However, significant  $\text{H}_2\text{O}_2$  decomposition occurs on the catalyst necessitating its usage in five-fold excess.

**KEYWORDS:**  $\text{CuCr}_2\text{O}_4$ , Spinel, Nanoparticles, Aniline, Azoxybenzene,  $\text{H}_2\text{O}_2$ , Oxidative coupling



## INTRODUCTION

The oxidation of aniline is an important reaction for the synthesis of its oxygenated derivatives such as hydroxylamine, nitroso, nitro, azo, and azoxy compounds.<sup>1</sup> Among these, the preparations of nitroso and azoxy compounds have attracted special importance as synthetically useful intermediates. Aromatic nitroso compounds are used in the vulcanization of rubber, stabilization of halogenated materials, and as antioxidants in lubricating oil,<sup>2–4</sup> whereas azoxybenzenes are employed as dyes, reducing agents, chemical stabilizers, and polymerization inhibitors. Some derivatives of azoxybenzenes are used as liquid crystals in electronic displays and therapeutic medicines.<sup>5</sup> Aromatic azo compounds are high-value chemicals widely used in the industry as dyes, pigments, food additives, and drugs.<sup>1,6–8</sup> A variety of oxidation methods using stoichiometric and catalytic routes have been reported. For example, arylamines can be oxidized with stoichiometric oxidants such as peracetic acid,<sup>9</sup>  $\text{MnO}$ ,<sup>10</sup>  $\text{Pb}(\text{OAc})_4$ ,<sup>11</sup>  $\text{Hg}(\text{OAc})_2$ ,<sup>12</sup> and  $\text{BaMnO}_4$ .<sup>13</sup> Various types of molecular sieves<sup>14,15</sup> and mesoporous silica containing nanometric dispersed titanium oxide have been reported for the oxidation of aniline to azoxybenzene.<sup>16</sup> It has been reported that mesoporous silicas containing cobalt oxide catalyst can be used for the selective oxidation of aniline to azoxybenzene using  $\text{H}_2\text{O}_2$  as the oxidant.<sup>17</sup> Recently, Li et al. reported synthesis of azobenzene using molecular oxygen in the liquid phase.<sup>18</sup> But in most of the cases, the recyclability of the catalysts and the product separation from the reaction mixtures become two major issues in liquid-phase reaction systems. Therefore, a recyclable catalyst that works under atmospheric pressure and comparatively low temperature is in high demand.

Copper chromite composite oxides have been used as catalysts for chemical reactions such as hydrogenation, dehydrogenation, oxidation, alkylation, and so forth and thus find wide commercial applications. Apart from its usage in chemical industries, copper chromite finds its major application as a burn rate modifier in solid propellant processing for space launch vehicles globally.<sup>19–21</sup> Although there are several reports for the preparation of copper chromite spinel catalysts,<sup>22–24</sup> self-assembled architectures with designed chemical components and tunable morphology remains a big challenge. Here, we report the preparation of a  $\text{CuCr}_2\text{O}_4$  spinel nanoparticle catalyst using cationic surfactant cetyltrimethylammonium chloride with the hydrothermal synthesis method for the oxidation of aniline to azoxy compounds. An aniline conversion of 78% with 92% selectivity of azoxybenzene was achieved at 70 °C using  $\text{H}_2\text{O}_2$  as the oxidant over the  $\text{CuCr}_2\text{O}_4$  spinel nanoparticle catalyst.

## EXPERIMENTAL SECTION

**Materials and Methods.**  $\text{CuCl}_2 \cdot 2\text{H}_2\text{O}$ ,  $\text{CrCl}_3 \cdot 6\text{H}_2\text{O}$ ,  $\text{NH}_3$  solution (20% aqueous solution), cetyltrimethylammonium chloride (CTAC), hydrazine solution (80% aqueous solution), aniline, and  $\text{H}_2\text{O}_2$  (50% aqueous solution) were purchased from Sigma Aldrich. All reagents were used as such without further purification. All solutions were prepared using doubled distilled water.

**Preparation of Catalyst.** The catalyst was prepared by modifying our own preparation method (Scheme S1, Supporting Information).<sup>25,26</sup> In a typical preparation method, 3.5 g of  $\text{CuCl}_2 \cdot 2\text{H}_2\text{O}$  and

Received: January 23, 2014

Revised: February 25, 2014

Published: March 3, 2014

Table 1. Physicochemical Properties of the  $\text{CuCr}_2\text{O}_4$  Spinel Nanoparticles Catalyst<sup>a</sup>

entry	catalyst	Cu/Cr molar ratio	BET surface area (m <sup>2</sup> /g)	morphology	particle size (nm)	
					XRD <sup>b</sup>	TEM
1	$\text{CuCr}_2\text{O}_4$ (fresh)	0.5	90.5	almost uniform dispersed particles with sizes of 25–50 nm	38	35
2	$\text{CuCr}_2\text{O}_4$ (spent, after five reuses)	0.5	91	almost uniform dispersed particles with sizes of 25–50 nm	37.5	36

<sup>a</sup>Estimated by ICP-AES. <sup>b</sup>Measured using Scherrer equation.

11 g of  $\text{CrCl}_3 \cdot 6\text{H}_2\text{O}$  at a desired molar ratio ( $\text{CuO}/\text{Cr}_2\text{O}_3 = 1$ ) were dissolved in 150 g of water to give a clear dark blue solution. The pH of the medium was made 8 by gradual addition of a  $\text{NH}_4\text{OH}$  solution dropwise; the color of the solution became greenish gradually. Then CTAC was dissolved in 30 mL water by intensive stirring for 2 h to form a gel. A solution of hydrazine monohydrate (80% aqueous solution) was added dropwise to the well-stirred mixture at RT by simultaneous vigorous agitation. All the reagents were used maintaining the ratio of  $\text{Cu}:\text{Cr}:\text{CTAC}:\text{hydrazine}:\text{H}_2\text{O} = 1:2:0.8:1.5:250$ . The mixture was stirred vigorously for 30 min and subsequently sealed in a Teflon-lined stainless steel autoclave (250 mL capacity). The autoclave was heated to and maintained at 200 °C for 18 h and then allowed to cool to RT. The green fluffy solid products (precipitates) were collected by centrifugation at 5000 rpm and washed with water and ethanol several times prior to drying in air at 100 °C for 6 h. The resulting dry powder was transferred to a quartz reactor inside a tubular resistance furnace for calcination. The calcination was operated at 700 °C in air at ramp of 1 °C min<sup>-1</sup>.

**Characterization Techniques.** Powder X-ray diffraction patterns were collected on a Bruker D8 advance X-ray diffractometer fitted with a Lynx eye high-speed strip detector and a  $\text{Cu K}\alpha$  radiation source. The line width of the XRD peak was taken for estimation of crystallite size by the Scherrer equation. Diffraction patterns in the 2–80° region were recorded at a rate of 0.5 degrees (2  $\theta$ ) per minute. Scanning electron microscopy images were taken on a FEI Quanta 200 F, using a tungsten filament doped with lanthanumhexaboride ( $\text{LaB}_6$ ) as an X-ray source, fitted with an ETD detector with high vacuum mode using secondary electrons, and an acceleration tension of 10 or 30 kV. Samples were analyzed by spreading them on a carbon tape to determine the particle size, shape, and morphology of the synthesized and commercial compounds. Energy dispersive X-ray spectroscopy was used in connection with SEM for the elemental analysis. The elemental mapping was also collected with the same spectrophotometer. TEM images were collected using a JEOL JEM 2100 microscope, and samples were prepared by mounting an ethanol-dispersed sample on a lacey carbon Formvar-coated Cu grid. The textural characterization of the sample was based on Brunauer–Emmett–Teller method using BET Belsorp equipment (BEL Japan, Inc.) by nitrogen adsorption at –196 °C. Prior to measurement, the sample was pretreated at 200 °C for 3 h under vacuum. X-ray photoelectron spectra were recorded on a Thermo Scientific K-Alpha X-ray photoelectron spectrometer. The resulting spectra were analyzed to identify the different oxidation states of the copper and chromium ions present in the sample. Prior to the analysis, the spectra were calibrated with reference to C1s observed at a binding energy of 284.5 eV. Chemical analyses of the metallic constituents were carried out by inductively coupled plasma atomic emission spectrometer (model PS 3000 uv, DRE, Leeman Laboratories, Inc., U.S.A.). Thermogravimetric analyses (TGA) of the uncalcined catalyst were carried out in a Pyris Diamond (Perkin-Elmer Instruments and Technology by SII, Seiko Instruments, Inc., USA) instrument balance by heating 2.15 mg samples at 5 °C min<sup>-1</sup> in a flowing air atmosphere.

**Liquid Phase Catalytic Reaction.** The catalytic reactions were carried out in a 50 mL round-bottomed flask with continuous stirring (1100 rpm). In a typical run, 0.05 g of catalyst was dispersed in a solution containing 1g of aniline, 3.7 g of  $\text{H}_2\text{O}_2$  (50% aqueous solution), and 10 mL of solvent (1, 4-dioxane). Aliquots were periodically collected every 1 h, centrifuged to remove the solid

particles, and analyzed by GC using a capillary column, HP5 (5% phenylmethylsiloxane (30 m  $\times$  0.25  $\mu\text{m}$ ), equipped with a FID detector. The identity of the products were established by GC and compared with the authentic products, GC-MS, and <sup>1</sup>H NMR. After completion of the reaction, the crude yield of the product was separated from the reaction mixture by workup and removing the solvent by rotavapor. The number of products in the crude yield was identified by TLC spots. After that, by means of column chromatography, the isolated yield of azoxybenzene was obtained, and the mass balance was estimated at the end of the experiment. The estimated error in analysis arising due to sampling and handling losses was between 3 and 5 mol %.

## RESULTS AND DISCUSSION

**Generation of  $\text{CuCr}_2\text{O}_4$  Spinel Nanoparticles.** We believe that the precursors of copper and chromium ionizes and counterions diffuse into the aqueous solution, maintaining the homogeneity of the medium. When concentration of the micelles was less than that in critical micelle concentration (CMC),  $\text{Cu}^{2+}$  and  $\text{Cr}^{3+}$  ions are preferentially located at the micellar surface due to the presence of  $\text{Cl}^-$  ions. The growth of the particles occurs along the side of the particles, which is exposed to water.<sup>27</sup> When the concentration of the surfactant becomes greater than or equal to CMC, the aqueous medium is largely populated by surfactant micelles. The Cu and Cr precursor ions approach toward the micellar headgroup region. In this situation, growth in a particular direction is prohibited due to the micellar steric effects, and the nanoparticles are allowed to grow to form spherical nanoparticles with limited size. The role of CTAC is prominent in basic medium (pH > 7),<sup>28</sup> and hydrazine forms complexes with  $\text{Cu}^{2+}$  ions,<sup>29</sup> thereby prohibiting the Ostwald ripening process to a certain extent (Scheme S1, Supporting Information). However, change in the concentration of any one of the gel components (Cu, Cr, CTAC, hydrazine) leads to the formation of the mixed metal oxides without forming the pure spinel phase,<sup>25</sup> and their respective morphologies can be distinguished from their SEM images (Figure S1, Supporting Information). This indicates that the mechanism for the generation of spinel phase with sizes 25–50 nm and its textural properties largely dependent on the gel composition.

**Catalyst Characterization.** The phase structure and purity of the as-synthesized sample were examined by powder X-ray diffraction (XRD) (Table 1). The XRD patterns of the Cu–Cr catalysts (Figure 1) showed the typical diffraction lines of the  $\text{CuCr}_2\text{O}_4$  spinel exclusively with the maximum intensity peak at a  $2\theta$  value of 35.2°, which is referred to the plane [311] (JCPDS 05-0657), with Cu and Cr occupying the tetrahedral and octahedral interstices, respectively. No characteristic peaks due to the impurities of the oxides of Cu or Cr and even phases corresponding to their metallic state were detected. The mean particle size was measured using the Scherrer equation, and it was found to be 35 nm, which matched well with the HRTEM

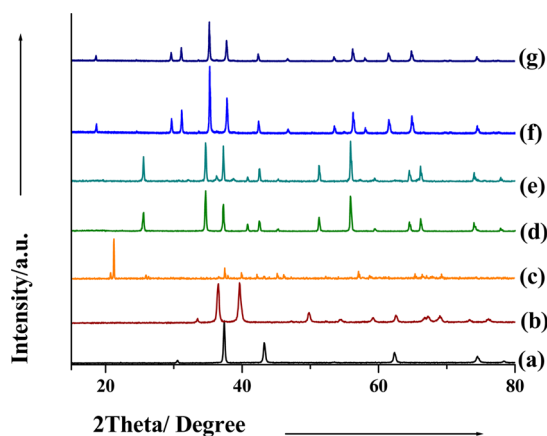


**Figure 1.** XRD patterns of (a) CuO, (b) Cu<sub>2</sub>O, (c) CrO<sub>3</sub>, (d) Cr<sub>2</sub>O<sub>3</sub>, (e) Cu/Cr<sub>2</sub>O<sub>3</sub><sup>imp</sup> (imp: impregnation method), (f) CuCr<sub>2</sub>O<sub>4</sub> (prepared catalyst), and (g) CuCr<sub>2</sub>O<sub>4</sub> (spent catalyst, after five reuses).

analysis. The representative SEM images of the catalyst are shown in Figure 2. The images show that an almost uniform

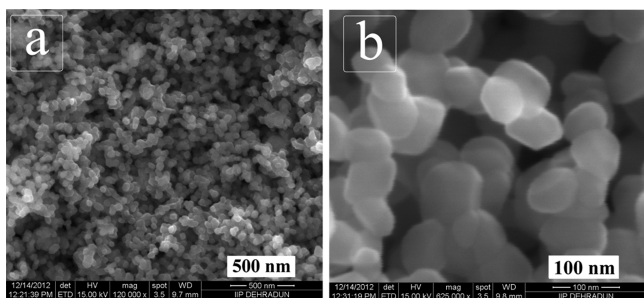


**Figure 2.** SEM images of the CuCr<sub>2</sub>O<sub>4</sub> spinel nanoparticle catalyst at (a) lower and (b) higher resolution.

particle size between 25 and 50 nm can be seen. Energy dispersive X-ray analysis (EDAX) showed the presence of Cu, Cr, and O in the sample (Figure S2, Supporting Information), and the distribution of the elements was carried out by means of elemental mapping (Figure S3, Supporting Information), which demonstrated the homogeneous distribution of Cu and Cr. TEM measurements were carried out to check the particle size and distribution of the particles and are shown in Figure 3. The particle sizes estimated from the TEM diagram were in good agreement with those obtained from the XRD data. A representative high-resolution TEM image is shown in Figure 3c, where the lattice fringes with a *d*-spacing of 0.30 nm corresponding to the spacing of the (211) plane of CuCr<sub>2</sub>O<sub>4</sub> can also be seen.<sup>20</sup> Furthermore, the TEM image of the spent catalyst (Figure 3d) shows that the topology and particle size of the catalyst were hardly changed even after five reuses. The particle size distribution histogram (Figure S4, Supporting Information) derived from the TEM image (Figure 3b) showed 10% of the particles having a size of 20 nm, 38% of the particles having a size of 30 nm, 25% of the particles having a size of 40 nm, and 10% of the particles having a size of 50 nm. The XPS spectra of Cu, Cr, and O in the CuCr<sub>2</sub>O<sub>4</sub> spinel are also presented. (Figure 4 and Figures S5 and S6, Supporting Information, respectively). The Cu2p spectrum of the fresh sample was characterized by two spin orbit doublets with strong satellite peaks. The Cu2p<sub>3/2</sub> signals fitted satisfactorily to two principal peak components at 935.2 and 933.8 eV. The BE for

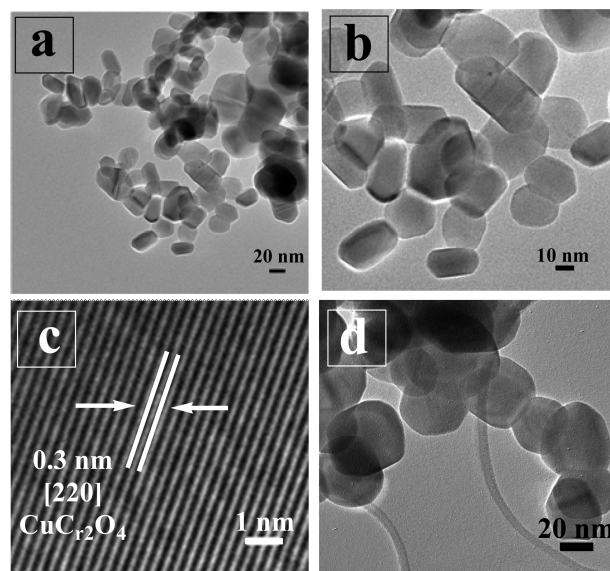


**Figure 3.** TEM images of (a–c) fresh and (d) spent CuCr<sub>2</sub>O<sub>4</sub> spinel nanoparticle catalyst.

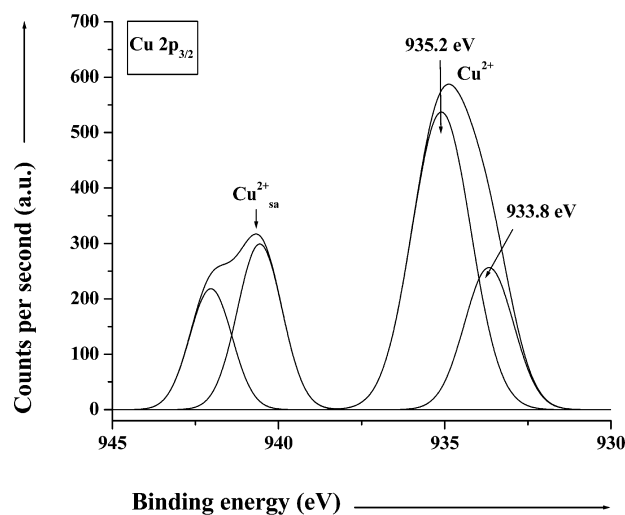


**Figure 4.** Cu 2p<sub>3/2</sub> core level spectra CuCr<sub>2</sub>O<sub>4</sub> spinel catalyst.

the Cu2p peak is in close agreement with that of CuCr<sub>2</sub>O<sub>4</sub>. The low energy component with Cu2p<sub>3/2</sub> with BE of 935.2 eV was associated to Cu<sup>2+</sup> in octahedral sites, whereas the high energy component with BE of 933.8 eV was due to Cu<sup>2+</sup> in the tetrahedral sites.<sup>30</sup> The Cr 2p<sub>3/2</sub> binding energies at 576.5 eV are typical of Cr<sup>3+</sup> and that of O1s occurred at 530.3 and 532.3 eV, revealing the presence of the O<sup>2-</sup> species at two different environments in CuCr<sub>2</sub>O<sub>4</sub> spinel.<sup>31</sup> The thermogravimetric analysis spectra of the uncalcined catalyst (Figure S7, Supporting Information) under an air atmosphere is presented over the temperature range from ambient to 500 °C. There was a continuous weight loss (~42%) due to the decomposition of the associated CTA molecules. Further weight loss was not observed when the temperature was further increased from 500 to 1000 °C, indicating the stability of the catalyst up to 1000 °C.

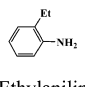
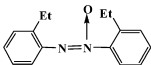
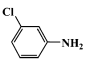
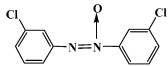
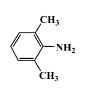
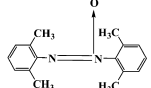
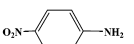
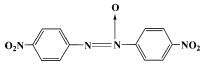
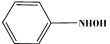
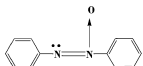
**Activity of the Catalyst.** The activity of the CuCr<sub>2</sub>O<sub>4</sub> spinel catalyst was examined for the direct transformation of azoxy compounds from anilines through the one-pot oxidative coupling reaction, and the results are summarized in Table 2.

Table 2. Reaction Conditions of Catalytic Oxidation of Aniline<sup>a</sup>

entry	catalyst	aniline conversion (%) <sup>b</sup>	azoxybenzene selectivity (%) <sup>c</sup>	yield of azoxybenzene (%) <sup>d</sup>	E <sub>o</sub> <sup>e</sup>
1	CuO <sup>COM</sup>	7.5	10	0.8	0.16
2	Cu <sub>2</sub> O <sup>COM</sup>	6.0	5	0.3	0.06
3	Cr <sub>2</sub> O <sub>3</sub> <sup>COM</sup>	8	9	0.7	0.15
4	CuCr <sub>2</sub> O <sub>4</sub> <sup>COM</sup>	15	40	6	0.3
5	CuO–Cr <sub>2</sub> O <sub>3</sub> <sup>IMP</sup>	2	15	0.3	0.06
6	CuO–Cr <sub>2</sub> O <sub>3</sub> <sup>CPM</sup>	6	10	0.6	0.13
7 <sup>f</sup>	CuO–Cr <sub>2</sub> O <sub>3</sub>	25	45	11.2	2.41
8 <sup>g</sup>	CuCr <sub>2</sub> O <sub>4</sub> <sup>NP</sup>	78	92	71.8	15.4
9 <sup>h</sup>	CuCr <sub>2</sub> O <sub>4</sub> <sup>NP</sup>	75.5	95.0	71.7	15.3
10 <sup>i</sup>	CuCr <sub>2</sub> O <sub>4</sub> <sup>WC</sup>	20	65	13.0	2.8
11	no catalyst	2.0	–	–	–

<sup>a</sup>Typical reaction conditions: solvent (1,4-dioxane) = 10 mL; substrate (aniline) = 1 g; catalyst = 0.05 g; aniline: H<sub>2</sub>O<sub>2</sub> (molar ratio) = 1:5; reaction temperature = 70 °C; and time = 10 h. <sup>b</sup>Conversion of aniline based upon the FID-GC using acetone as external standard = [moles of aniline reacted/initial moles of aniline used] × 100. <sup>c</sup>Selectivity to azoxybenzene = [moles of azoxybenzene produced/moles of aniline reacted] × 100. <sup>d</sup>Yield of azoxybenzene = conversion × selectivity/100. <sup>e</sup>E<sub>o</sub> = H<sub>2</sub>O<sub>2</sub> efficiency = [moles of azoxybenzene formed/total moles of H<sub>2</sub>O<sub>2</sub> added] × 100. <sup>f</sup>Cu-nanoclusters supported on Cr<sub>2</sub>O<sub>3</sub>. <sup>g</sup>Prepared CuCr<sub>2</sub>O<sub>4</sub> spinel nanoparticles and <sup>h</sup>catalyst after five reuses. <sup>i</sup>CuCr<sub>2</sub>O<sub>4</sub><sup>WC</sup>: catalyst prepared without using CTAC. COM: commercial. IMP: impregnation method. CPM: coprecipitation method.

Table 3. Formation of Azoxybenzenes via Oxidation of Anilines<sup>a</sup>

Entry	Anilines	Products (Azoxybenzenes)	Conversion of Anilines (%) <sup>b</sup>	Selectivity of Product (%) <sup>c</sup>	Yield of Product (%) <sup>d</sup>
1	 2-Ethylaniline		88	97	85.3
2	 3-Chloroaniline		85	95.5	81.1
3	 2,6-Dimethylaniline		87	84	73.0
4	 4-Nitroaniline		70	85	59.5
5	 Phenyl hydroxyl amine		>99	>99	99

<sup>a</sup>Typical reaction conditions: solvent(1,4-dioxane) = 10 mL; substrate = 1 g; catalyst = 0.05 g; aniline: H<sub>2</sub>O<sub>2</sub> (molar ratio) = 1:5; reaction temperature = 70 °C; and time = 10 h.

1,4-Dioxane was chosen as the solvent. When H<sub>2</sub>O<sub>2</sub> (3.7 g) was added to a solution of aniline (1 g) and 0.05 g of CuCr<sub>2</sub>O<sub>4</sub> spinel catalyst in 1,4-dioxane (10 mL) under normal atmospheric pressure at RT (25 °C), negligible azoxybenzene (6%) was obtained (Figure S8, Supporting Information). While

optimizing the reaction conditions, we found that the yield of the desired product (azoxybenzene) increased by increasing the reaction temperature (Figure S8, Supporting Information).<sup>3</sup> However, the use of excess H<sub>2</sub>O<sub>2</sub> did not increase the yield (Figure S9, Supporting Information) presumably because of the

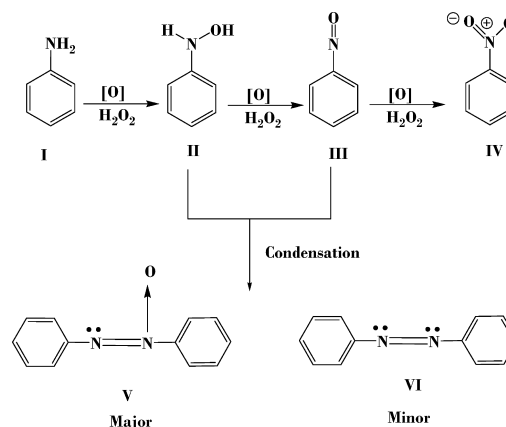
formation of other products. We performed the blank experiment (entry 11, Table 2), which showed no activity, indicating the necessity of the catalyst, and with the increment of the weight of the catalyst, the increment in the conversion of aniline was observed. Although with further increment in catalyst weight (>0.05 g) conversion of aniline was increased, selectivity to azoxybenzene decreased rapidly due to the formation of polymerized products (Figure S11, Supporting Information). Notably, conventional and commercial catalysts (entries 1–6, Table 2) also showed very poor activity toward the oxidative coupling reaction of aniline. So, the essence of the spinel particle catalyst was proved. The higher activity of the spinel nanoparticles can be attributed to its accessible surfaces toward the substrate molecules owing to their greater surface/volume ratio compared to that of the commercial catalyst, which possesses particles with irregular shapes and larger sizes (Figure S1d, Supporting Information). Furthermore, to elucidate the role of the nanosize effect, the  $\text{CuCr}_2\text{O}_4$  spinel nanoparticle catalyst was substituted by the  $\text{CuCr}_2\text{O}_4$  catalyst with larger particle sizes (prepared without using CTAC) (Figure S1b, Supporting Information) at the optimum reaction conditions. The yield of the product was very poor, indicating the fact that the size of the particle has a marked influence on the reactivity of the catalysts (entry 10, Table 2). With increments in temperature, time, or even concentration of  $\text{H}_2\text{O}_2$ , polymerized products were noticed considerably, leading to a decrease in selectivity to azoxybenzene.<sup>32–34</sup> The decrement in the activity of the catalyst can be attributed probably to the fact that the so-produced polymers mask the catalyst surface and thereby prevent it from interacting with the substrate molecules.

The oxidant,  $\text{H}_2\text{O}_2$ , was used in an excess amount (aniline:  $\text{H}_2\text{O}_2 = 1:5$  molar ratio). In general,  $\text{H}_2\text{O}_2$  decomposes spontaneously over a catalytic surface. We did a  $\text{H}_2\text{O}_2$  decomposition test with our catalyst (absence of aniline and solvent) and found that greater than 80% of the  $\text{H}_2\text{O}_2$  decomposed at the reaction temperature. Hence, we used an excess of  $\text{H}_2\text{O}_2$ , so that the active oxygen species needed for the oxidation of aniline could be available during the reaction. Furthermore, we took the reaction mixture and performed permanganometric titrations to detect  $\text{H}_2\text{O}_2$ , but no  $\text{H}_2\text{O}_2$  was discovered in the reaction mixture, indicating that the unreacted  $\text{H}_2\text{O}_2$  molecules have been decomposed completely. We have plotted  $\text{H}_2\text{O}_2$  consumption in terms of its efficiency ( $E_o$ ) in Table 2.

The optimum reaction condition of the oxidative coupling reaction was applied on various substituted anilines (Table 3). The reaction was remarkably selective for the azoxybenzene product regardless of the presence of the electron donor or acceptor groups in the phenyl ring. But conversion of the reactant (*p*-nitroaniline) was somewhat less compared to the other substrates in Table 3. The reason may be attributed to the presence of a strongly electron-withdrawing nitro group at the para position that hinders the substrate conversion (entry 4, Table 3). Furthermore, 2,6-dimethyl aniline did not furnish a high yield presumably because of steric hindrance of the substrate.

**Reaction Mechanism.** The oxidative coupling of aniline over a  $\text{CuCr}_2\text{O}_4$  spinel nanoparticle catalyst is believed to follow the path as illustrated in Scheme 1. Oxidation of aniline produces phenyl hydroxylamine (II) and nitrosobenzene (III). Condensation of (II) and (III) produces azoxybenzene (V) over the catalyst surface. Furthermore, some unreacted aniline

Scheme 1. Oxidative Coupling of Aniline



molecules also react with (II) to produce azobenzene (VI) as a side product. When phenylhydroxyl amine was introduced to react under the same conditions, azoxybenzene was produced exclusively (entry 4, Table 3), which supports the stated mechanism for the oxidative coupling reaction of aniline. It is worth mentioning that the condensation reaction occurred over the catalyst surface and not spontaneously in the solution mixture; furthermore, the process ruled out the possibility of a side reaction apart from the oxidative coupling of aniline.

**Reusability Test.** At the end of the reaction, the catalyst was filtered in the hot condition and was dried for 12 h at 100 °C and used without regeneration. Recycling and reusability of the catalyst was examined by introducing the used catalyst subsequently five times to carry out the catalytic oxidation. The catalyst showed about a 72% yield even after five successive runs (Figure S12, Supporting Information). For each of the five runs, the resulting filtrate was independently analyzed by inductively coupled plasma (ICP) and atomic absorption spectroscopy for free or dissolved metal ions, and only trace amounts of  $\text{Cu}^{2+}$  (<3 ppb) were detected after the fifth run. We performed the catalytic activity of the filtrate after the fifth run and found that the activity is negligible. We also used  $\text{Cu}^{2+}$  solution and performed the catalytic activity (homogeneous catalyst) and also found that the activity is almost zero. These results indicated that the spinel phase is the active species.

The amount of Cu and Cr present in the catalyst was almost the same as that of the fresh catalyst (as estimated by ICP-AES). This experiment confirms that the catalyst possesses a truly heterogeneous nature.

## CONCLUSIONS

In conclusion, we have demonstrated the surfactant-mediated hydrothermal preparation of a  $\text{CuCr}_2\text{O}_4$  spinel nanoparticle catalyst, and the catalyst showed very good performance for the selective oxidation of aniline to azoxybenzene. The catalyst was characterized by XRD, XPS, SEM, TEM, TGA, and ICP-AES in detail. HRTEM analysis showed that the catalyst is comprised of uniform particles with sizes of about 35 nm. An aniline conversion of 78%, with 92% selectivity to azoxybenzene, can be achieved at 70 °C with  $\text{H}_2\text{O}_2$  as the oxidant. The catalyst did not show any leaching after five reuses, confirming its true heterogeneity. This newly developed  $\text{CuCr}_2\text{O}_4$  spinel nanoparticle catalyst may serve as a potential catalyst for the preparation of azoxybenzene from aniline in a single step.

## ■ ASSOCIATED CONTENT

### ● Supporting Information

Schematic presentation of catalyst preparation, SEM, XPS plots, effect of different reaction parameters on aniline oxidation reaction etc. This material is available free of charge via the Internet at <http://pubs.acs.org>.

## ■ AUTHOR INFORMATION

### Corresponding Author

\*Fax: +91 1352660202. Tel: +91 135 2525 917. E-mail: [raja@iip.res.in](mailto:raja@iip.res.in).

### Notes

The authors declare no competing financial interest.

## ■ ACKNOWLEDGMENTS

S.S.A. thanks CSIR and S.G. thanks UGC, New Delhi, India, for their respective fellowships. R.B. thanks CSIR, New Delhi, for financial support in the form of the 12 FYP Project (CSC-0125). The Director of CSIR-IIP is acknowledged for his help and encouragement. The authors thank Analytical Section Division, IIP, for the analytical services.

## ■ ABBREVIATIONS

CTAC, cetyltrimethylammonium chloride; XPS, X-ray photoelectron spectroscopy; XRD, X-ray diffraction; SEM, scanning electron microscopy; TEM, transmission electron microscopy; TGA, thermogravimetric analysis

## ■ REFERENCES

- (1) Catino, S. C.; Farris, E. *Concise Encyclopedia of Chemical Technology*; John Wiley & Sons: New York, 1985; Chapter 7.
- (2) Gowenlock, B. G.; Lüttke, W. Structure and properties of C-nitroso-compounds. *Q. Rev. Chem. Soc.* **1958**, *12*, 321–340.
- (3) Zengel, H. G. New industrially feasible process for the production of nitrosoaniline. *Chem. Ing. Tech.* **1983**, *55*, 962–963.
- (4) Selvam, T.; Ramaswamy, A. V. A new method for the selective oxidation of aniline to nitrosoaniline over titanium silicate molecular sieves, TS-1, using H<sub>2</sub>O<sub>2</sub> as oxidant. *Chem. Commun.* **1996**, 1215–1216.
- (5) Sakuae, S.; Tsubakino, T.; Nishiyama, Y.; Ishii, Y. Oxidation of aromatic amines with hydrogen peroxide catalyzed by cetylpyridinium heteropolyoxometalates. *J. Org. Chem.* **1993**, *58*, 3633–3638.
- (6) Egli, R. *Colour Chemistry: The Design and Synthesis of Organic Dyes and Pigments*; Peter, A. T., Freeman, H. S., Eds.; Elsevier: London, 1991; Chapter 7.
- (7) Venkataraman, K. *The Chemistry of Synthetic Dyes*; Academic Press: London, 1970; Chapter 6.
- (8) Gurrane, A.; Corma, A.; Garcia, H. Gold-catalyzed synthesis of aromatic azo compounds from anilines and nitroaromatics. *Science* **2008**, *322*, 1661–1664.
- (9) White, R. W.; Emmons, W. D. The chemistry of permaleic acid. *Tetrahedron* **1962**, *17*, 31–34.
- (10) Wheeler, O. H.; Gonzalez, D. Oxidation of primary aromatic amines with manganese dioxide. *Tetrahedron* **1964**, *20*, 189–193.
- (11) Baumgarten, H. E.; Staklis, A.; Miller, E. M. Reactions of amines. XIII. The oxidation of N-Acyl-N-arylhydroxylamines with lead tetracetate. *J. Org. Chem.* **1965**, *30*, 1203–1206.
- (12) Wenkert, E.; Wickberg, B. General methods of synthesis of indole alkaloids. II. A flavopereirine synthesis. *J. Am. Chem. Soc.* **1962**, *84*, 4914–4919.
- (13) Firouzabadi, H.; Mostafavipoor, Z. Barium manganate. A versatile oxidant in organic synthesis. *Bull. Chem. Soc. Jpn.* **1983**, *56*, 914–917.

(14) Waghmode, S. B.; Sabne, S. M.; Sivasankar, S. Liquid phase oxidation of amines to azoxy compounds over ETS-10 molecular sieves. *Green Chem.* **2001**, *3*, 285–288.

(15) Tuel, A.; Hubert-Pfalzgraf, L. G. Nanometric monodispersed titanium oxide particles on mesoporous silica: synthesis, characterization, and catalytic activity in oxidation reactions in the liquid phase. *J. Catal.* **2003**, *217*, 343–353.

(16) Jagtap, N.; Ramaswamy, V. Oxidation of aniline over titania pillared montmorillonite clays. *Appl. Clay Sci.* **2006**, *33*, 89–98.

(17) Chang, C. F.; Liu, S. T. Catalytic oxidation of anilines into azoxybenzenes on mesoporous silicas containing cobalt oxide. *J. Mol. Catal. A: Chem.* **2009**, *299*, 121–126.

(18) Cai, S.; Rong, H.; Yu, X.; Liu, X.; Wang, D.; He, W.; Li, Y. Room temperature activation of oxygen by monodispersed metal nanoparticles: Oxidative dehydrogenative coupling of anilines for azobenzene syntheses. *ACS Catal.* **2013**, *3*, 478–486.

(19) Adkins, H.; Connor, R. The catalytic hydrogenation of organic compounds over copper chromite. *J. Am. Chem. Soc.* **1931**, *53*, 1091–1095.

(20) Kawamoto, A. M.; Pardini, L. C.; Rezende, L. C. Synthesis of copper chromite catalyst. *Aerosol Sci. Technol.* **2004**, *8*, 591–598.

(21) Sathiskumar, P. S.; Thomas, C. R.; Madras, G. Solution combustion synthesis of nanosized copper chromite and its use as a burn rate modifier in solid propellants. *Ind. Eng. Chem. Res.* **2012**, *51*, 10108–10116.

(22) Connor, R.; Folkers, K.; Adkins, H. The preparation of copperchromium oxide catalysts for hydrogenation. *J. Am. Chem. Soc.* **1932**, *54*, 1138–1145.

(23) Roy, S.; Ghose, J. Synthesis and studies on some copper chromite spinel oxide composites. *Mater. Res. Bull.* **1999**, *34*, 1179–1186.

(24) Armstrong, R. W.; Baschung, B.; Booth, D. W. Enhanced propellant combustion with nanoparticles. *Nano Lett.* **2003**, *3*, 253–255.

(25) Sarkar, B.; Prajapati, P.; Tiwari, R.; Tiwari, R.; Ghosh, S.; Acharyya, S. S.; Pendem, C.; Singha, R. K.; Konathala, L. N. S.; Kumar, J.; Sasaki, T.; Bal, R. Room temperature selective oxidation of cyclohexane over Cu-nanoclusters supported on nanocrystalline Cr<sub>2</sub>O<sub>3</sub>. *Green Chem.* **2012**, *14*, 2600–2606.

(26) Acharyya, S. S.; Ghosh, S.; Tiwari, R.; Sarkar, B.; Singha, R. K.; Pendem, C.; Sasaki, T.; Bal, R. Preparation of CuCr<sub>2</sub>O<sub>4</sub> spinel nanoparticles catalyst for selective oxidation of toluene to benzaldehyde. *Green Chem.* **2014**, DOI: 10.1039/C3GC42369G.

(27) De, S.; Mandal, S. Surfactant-assisted shape control of copper nanostructures. *Colloids Surf., A* **2013**, *421*, 72–83.

(28) Hashempour, M.; Razavizadeh, H.; Rezaie, H.; Hashempour, M.; Ardestani, M. Chemical mechanism of precipitate formation and pH effect on the morphology and thermochemical co-precipitation of W–Cu nanocomposite powders. *Mater. Chem. Phys.* **2010**, *123*, 83–90.

(29) Heaton, B. T.; Jacob, C.; Page, P. Transition metal complexes containing hydrazine and substituted hydrazines. *Coord. Chem. Rev.* **1996**, *154*, 193–229.

(30) Pantaleo, G.; Liotta, L. F.; Venezia, A. M.; Deganello, G.; Ezzo, E. M.; El Kherbawi, M. A.; Atia, H. Support effect on the structure and CO oxidation activity of Cu–Cr mixed oxides over Al<sub>2</sub>O<sub>3</sub> and SiO<sub>2</sub>. *Mater. Chem. Phys.* **2009**, *114*, 604–611.

(31) Severino, F.; Brito, J. L.; Laine, J.; Fierro, J. L. G.; López Agudoy, A. Nature of copper active sites in the carbon monoxide oxidation on CuAl<sub>2</sub>O<sub>4</sub> and CuCr<sub>2</sub>O<sub>4</sub> spinel type catalysts. *J. Catal.* **1998**, *177*, 82–95.

(32) Sapurina, I.; Stejskal, J. The mechanism of the oxidative polymerization of aniline and the formation of supramolecular polyaniline structures. *Polym. Int.* **2008**, *57*, 1295–1325.

(33) Bicak, N.; Karagoz, B. Polymerization of aniline by copper-catalyzed air oxidation. *J. Polym. Sci., Part A: Polym. Chem.* **2006**, *44*, 6025–6031.

(34) Franco, A. Azoxy Containing Polyamide Polymers. U.S. Patent US3642709 A, 1972.